Interaction of adsorbates with electric field fluctuations near surfaces: Influence of the STM tip and plasmonic effects

Ping Chu* and D. L. Mills†

Department of Physics and Astronomy, University of California–Irvine, Irvine, California 92697, USA
(Received 8 January 2009; published 25 March 2009)

We discuss the interaction of adsorbates with fluctuating electric fields produced by zero-point charge fluctuations of electrons in the substrate. Zero-point motions associated with surface or interface plasmons are a source of such electric field fluctuations. When an adsorbate is on an oxidized surface, direct hybridization of the adsorbate electrons with those in the substrate can be ignored, and the long-ranged Coulomb field provides coupling of the adsorbate's electrons to those in the substrate through the electric field fluctuations. Earlier we developed a formalism that allows one to calculate adsorbate energy-level shifts along with the nonradiative lifetime of excited states with origin in these interactions. The present paper explores the influence of a nearby STM tip on the spectrum of electric field fluctuations. We also describe studies of the energy-level shifts of a Mg porphine molecule on the oxidized NiAl (110) surface, along with the nonradiative lifetime of its LUMO+1 state. The dependence of these effects on the distance between the tip and the oxide layer is studied. We find good agreement with data on the nonradiative lifetime of the LUMO+1 state of this molecule, along with its tip-induced shift in energy.

I. INTRODUCTION

There is great interest currently in the use of the scanning tunneling microscope (STM) to study the vibrational and electronic properties of isolated adsorbates on surfaces.[1–3] In our view, it is truly remarkable that with this technique one may study selected, individual atoms and explore the vibrational or electronic response of molecules by probing selected points inside the molecule. It is also possible to directly inject electrons into excited states through use of the STM, and then explore the response of a molecule to a single added electron.[4,5] One may measure directly the width of the excited state, detect the single photon emitted when a transition is made back to the ground state, and explore other issues as well.

If one is interested in excited state properties, and the adsorbed molecule or atom is chemisorbed directly onto a metal surface, then the width of the excited states can be very large. There is direct hybridization between the electrons in excited state with the substrate electrons, with the consequence that the nonradiative lifetime is very short indeed, by virtue of direct coupling to particle hole pairs. Under these conditions, it is impossible to resolve vibronic features in the emission spectrum, or to study other fine structure in the spectrum of excited states.

This problem may be resolved by growing a thin oxide layer on the surface.[6] The adsorbate then resides on the oxide, and direct hybridization between the molecule and the substrate electrons is very small so its influence can be neglected, to excellent approximation. To appreciate that this is so, we have seen in an earlier paper[7] that the electronic energy-level positions calculated for a Mg porphine molecule placed in free space are in good accord with those reported in Ref. 4. In this experiment, the Mg porphine molecule was placed on an oxidized NiAl(110) surface.

Even though one can set aside effects of direct hybridization between the adsorbate and the substrate electrons in the circumstance just described, interactions between the adsorbate electrons and substrate electrons still exist and play an important role in influencing the electronic properties of the adsorbate. One begins by noting that there are necessarily zero-point fluctuations in the charge density within the substrate. If the substrate surface is such that it supports well defined surface plasmons, then the zero-point fluctuations associated with these modes are one portion of the total spectrum of charge fluctuations, which extend down to zero frequency if the substrate is metallic in nature. The zero-point charge motions set up fluctuating electric fields in the vacuum above the substrate, and the adsorbate electrons are influenced by them. In an earlier paper,[7] a general many-body description was developed of the contribution to the proper self-energy of electrons in an adsorbate near a surface outside of which such zero-point fluctuations exist. The real part of the self-energy describes energy-level shifts that result from this interaction, and the imaginary part provides one with the contribution to the nonradiative decay rate of excited states associated with excitation of particle hole pairs in the substrate. If the excited state falls into the appropriate energy range, the decay will be to surface plasmons. The energy-level shifts that result from this coupling can be appreciable, as we shall see from the calculations presented in this paper. In Ref. 7, it was proved that if one extracts from the formalism the energy-level shift of a "sterile electron," the shift reduces to precisely the image potential energy of a point charge near a surface. The term "sterile electron" refers to an electron trapped in a highly localized state a certain distance z_0 above the surface, with no excited states present. In a real system, the wave function is not localized, and in addition, the dynamic fluctuations in the electric fields near the surface produce energy-level shifts associated with virtual transitions to excited states. We refer to the energy-level shift in this circumstance as a dynamic image potential shift.

Such effects are not included in standard density-functional studies of adsorbates, so energy-level positions

calculated in density-functional theory should be adjusted with corrections generated by a scheme such as we employ here. It is the case that image potential effects have been incorporated into studies of metallic surfaces.[8] However, to date there have been no calculations reported which incorporate the image potential into the description of electronic properties of adsorbates, so far as we know. To do this remains a challenge for density-functional theory. In our approach, the electric field fluctuations, which are fully quantum mechanical in nature, are described through use of a method that replaces the tip/substrate/oxide layer combination by dielectric media. Within this scheme we may carry out quantitative calculations for real material combinations by making use of their optical dielectric constants. Such an approach was developed some years ago to provide a description of electron-energy-loss spectra (EELS) of surfaces in the dipole scattering regime.[9] This dielectric formulation of EELS, very similar in physical content to the approach in Ref. 7, accounts nicely for electron-energy-loss data even when small length scales are probed. An example is the influence of a monolayer of Ag on the electron-energy-loss spectrum of a GaAs surface.[10] A complete theory, of course, would resort to a fully microscopic description of the charge fluctuations and thus would be quite correct when truly microscopic length scales are addressed. However, such an analysis is not yet possible for structures such as those explored in Ref. 7 and in the present paper.

In Ref. 7, calculations were presented of the energy-level shifts of the states of a Mg porphine molecule placed on an oxidized NiAl surface. In addition, the contribution to the nonradiative decay rate from the mechanism described above was also calculated for the LUMO+1 state of this molecule.[11] These calculations did not include the influence of the STM tip on the spectrum of charge fluctuations near the substrate. As the tip approaches the molecule, it is the case that surface plasmons localized near the tip couple to those localized on the metallic substrate, to produce collective modes of the tip/substrate combination.[12] Thus, in fact both the fluctuation-induced energy-level shifts and the nonradiative lifetime of excited states will depend on the tip/substrate separation. The purpose of this paper is to develop a method for describing such tip-induced effects. We then present theoretical studies for the Mg porphine molecule adsorbed on an oxidized NiAl surface. We present results for tips fabricated from various materials. We remark that our calculated nonradiative lifetime for the LUMO+1 state is rather close to the value reported in Refs. 5 and 24, and this is true as well of tip-induced shifts in the energy of the LUMO+1 state as well. These results establish, in our view, the conclusion that field fluctuations such as explored here indeed play a key role in the electronic properties of substrates, and also the proximity of an STM tip to an adsorbate influences its electronic properties.

The outline of this paper is as follows. In Sec. II, we provide a brief review of the theoretical results of Ref. 7, and we then show how the influence of the tip may be incorporated into the theory. We present our numerical results in Sec. III and concluding remarks are in Sec. IV.

II. THEORETICAL FORMALISM

We begin with a brief summary of the formalism developed in Ref. 7. We refer the reader to this paper for a detailed derivation of the results summarized here.

We consider an atom or a molecule in close proximity to surfaces of some structure of interest, and as discussed in Sec. I we ignore direct hybridization between the electrons in the adsorbate and those bound in the surrounding structure. This may be a simple plane surface, possibly oxidized, such as considered in the explicit calculations of Ref. 7, or a more complex geometry. The Hamiltonian of the system is then written

$$H = H_a + H_M + V, \tag{1}$$

where H_a describes the electrons in the adsorbate, H_M those in the metallic substrate, and V the interaction between the two sets of electrons through the electric field fluctuations discussed in Sec. I. The fermion field operator that describes the electronic system is written as $\psi(\vec{r}) = \psi_a(\vec{r}) + \psi_M(\vec{r})$, where the first term is the annihilation operator for the electrons in the adsorbate, and the second term that in the surrounding structure. We shall write $\psi_a(\vec{r}) = \sum_\alpha c_\alpha \varphi_\alpha(\vec{r})$ and $H_a = \sum_\alpha \varepsilon_\alpha c_\alpha^+ c_\alpha$, where the collection $\{\varphi_\alpha(\vec{r})\}$ are orbitals generated from an electronic structure calculation, and $\{\varepsilon_\alpha\}$ are the associated energy levels. We shall not need a precise form for H_M. The interaction V is given by

$$V = e \int d^3 r \, \psi_a^+(\vec{r}) \Phi(\vec{r}) \psi_a(\vec{r}), \tag{2a}$$

where $\Phi(\vec{r})$ is the operator (in the Schrodinger representation) corresponding to the electrostatic potential associated with the electric field fluctuations. One has the explicit form

$$\Phi(\vec{r}) = e \int_V d^3 r' \frac{\psi_M^+(\vec{r'}) \psi_M(\vec{r'})}{|\vec{r} - \vec{r'}|}, \tag{2b}$$

where the spatial integration is over the region which contains the electrons of the surrounding structure.

We proceed by introducing a many-body Green's function which describes the electrons in the adsorbate (we use units where $\hbar = 1$):

$$G_a(\vec{r}, t; \vec{r'}, t') = -i \langle T[\psi_a(\vec{r}, t) \psi_a^+(\vec{r'}, t')] \rangle. \tag{3}$$

Here T is the standard time ordering operator of many-body theory, and in what follows operators with time dependence are in the Heisenberg representation. In Ref. 7 it is argued that this object obeys a Dyson equation that has the form

$$\left(i \frac{\partial}{\partial t} - H_a \right) G_a(\vec{r}, t; \vec{r'}, t')$$

$$- \int d^3 r'' dt'' \Sigma(\vec{r}, t; \vec{r''}, t'') G_a(\vec{r''}, t''; \vec{r'}, t')$$

$$= \delta(\vec{r} - \vec{r'}) \delta(t - t'), \tag{4}$$

where to the lowest order in the interaction V the proper self-energy has the form

$$\Sigma(\vec{r},t;\vec{r}',t') = -e^2 G_a^{(0)}(\vec{r},t;\vec{r}',t')\langle T[\Phi(\vec{r}',t')\Phi(\vec{r},t)]\rangle, \quad (5)$$

where $G_a^{(0)}(\vec{r},t;\vec{r}',t')$ is the adsorbate Green's function in the limit V is set to zero.

The proper self-energy is a function of only $t-t'$, and we make a Fourier transform with respect to this variable. The Fourier transformed proper self-energy is then given by, with ε the frequency variable,

$$\Sigma(\vec{r},\vec{r}';\varepsilon) = -\frac{e^2}{2\pi}\sum_\alpha \varphi_\alpha(\vec{r})\varphi_\alpha(\vec{r}')^*$$
$$\times \left[\int_{-\infty}^{\infty} \frac{d\omega(1-f_\alpha)\rho_{\Phi\Phi}(\vec{r}',\vec{r};\omega)}{(\varepsilon - \varepsilon_\alpha - \omega + i\eta)} \right.$$
$$\left. + \int_{-\infty}^{\infty} \frac{d\omega f_\alpha \rho_{\Phi\Phi}(\vec{r},\vec{r}';\omega)}{(\varepsilon - \varepsilon_\alpha + \omega - i\eta)} \right], \quad (6)$$

where f_α is unity if orbital α is occupied and zero if it is empty. In this section, all formulae given are for the zero temperature. The function $\rho_{\Phi\Phi}(\vec{r},\vec{r}';\omega)$ is the spectral density function which describes, in essence, the frequency spectrum of the fluctuations in the electrostatic potential. When $\vec{r}=\vec{r}'$, this function describes the frequency spectrum of electrostatic potential fluctuations at the point $\vec{r}$. We have assumed the temperature T is zero, so these are zero-point fluctuations. The generalization to finite temperatures is commented in Ref. 7. Since the physical effects of interest in the present paper involve fluctuations whose frequency satisfies $\hbar\omega \gg k_B T$ the zero-temperature limit is all we require here.

The adsorbate Green's function may also be Fourier transformed with respect to the variable $t-t'$ and we may write its Fourier transform in the form

$$G_a(\vec{r},\vec{r}';\varepsilon) = \sum_{\alpha,\alpha'} \varphi_\alpha(\vec{r})\varphi_{\alpha'}(\vec{r}')^* g_{\alpha\alpha'}(\varepsilon). \quad (7)$$

In Ref. 7, it is demonstrated that to the lowest order in V one has

$$g_{\alpha\alpha'}(\varepsilon) = \delta_{\alpha,\alpha'}/[\varepsilon - \varepsilon_\alpha - \Sigma_{\alpha\alpha'}(\varepsilon)], \quad (8)$$

where

$$\Sigma_{\alpha\alpha}(\varepsilon_\alpha) = -\frac{e^2}{2\pi}\int_0^\infty d\omega \int d^3r d^3r' \rho_{\Phi\Phi}(\vec{r},\vec{r}';\omega) \sum_\beta \varphi_\alpha^*(\vec{r})\varphi_\beta(\vec{r})$$
$$\times \left[\frac{1-f_\alpha}{\varepsilon_\alpha - \varepsilon_\beta - \omega + i\eta} \right.$$
$$\left. + \frac{f_\alpha}{\varepsilon_\alpha - \varepsilon_\beta + \omega - i\eta} \right] \varphi_\alpha(\vec{r}')\varphi_\beta^*(\vec{r}'). \quad (9)$$

Again to the lowest order in V, the shift in the excitation energy of orbital α which results from the field fluctuations is given by $\mathrm{Re}[\Sigma_{\alpha\alpha}(\varepsilon_\alpha)]$ whereas the nonradiative decay rate of an excited state is found from $\mathrm{Im}[\Sigma_{\alpha\alpha}(\varepsilon_\alpha)]$. In regard to the level shifts, the reader should keep in mind the fact that the Green's functions describe excitation energies. Thus, if $\mathrm{Re}[\Sigma_{\alpha\alpha}(\varepsilon_\alpha)]$ is positive for an occupied orbital, this corre-

sponds to a downward shift in energy of the orbital, since it describes an increase in the excitation energy of the hole formed by removing an electron from the orbital.

So far our discussion is quite general, and we have not had the need to specify the geometry of the structures which surround the adsorbate, nor have we had the need to specify how we calculate the frequency spectrum of the field fluctuations. Our only assumption has been that we can ignore direct hybridization between the orbitals of the adsorbate and, of course, we assume also that the influence of the coupling of the adsorbate electrons to the fluctuations may be treated to the lowest order in V.

What we need next is the means to calculate the spectral density of the potential fluctuations, as described by $\rho_{\Phi\Phi}(\vec{r},\vec{r}';\omega)$. In Ref. 7, we have adapted the elegant physical picture set forth in Ref. 13. Here it is demonstrated that if one can describe the system of interest through complex, frequency-dependent dielectric constants, then the quantum theoretic field fluctuation spectrum may be directly related to appropriate Green's functions associated with classical electromagnetic theory. As in Ref. 7, we proceed within this framework. We replace the structures of interest by dielectric materials each described by the appropriate complex frequency dependent dielectric constants $\epsilon(\omega)$. We take the surfaces to be sharp discontinuities so our results do not apply to the atomic length scale, strictly speaking. However, we will apply the theory to geometries where some lengths involved are rather small, noting as mentioned earlier that EELS theories carried out on this basis provide quite a satisfactory account of data on systems where the length scales encountered are quite small.[9,10] The virtue of this approach is that we can then carry out calculations for diverse material combinations with knowledge of only their optical dielectric constants.

We then proceed as follows. We introduce a classical Green's function, $D_{\Phi\Phi}(\vec{r},\vec{r}';\omega+i\eta)$ that describes the response of the structure of interest to a unit point charge placed at position $\vec{r}$:

$$\vec{\nabla} \cdot [\epsilon(\vec{r},\omega+i\eta)\vec{\nabla}D_{\Phi\Phi}(\vec{r},\vec{r}';\omega+i\eta)] = -4\pi\delta(\vec{r}-\vec{r}'). \quad (10)$$

We then have the relation[7,13]

$$\rho_{\Phi\Phi}(\vec{r},\vec{r}';\omega) = i\{D_{\Phi\Phi}(\vec{r},\vec{r}';\omega+i\eta) - D_{\Phi\Phi}(\vec{r}',\vec{r};\omega+i\eta)^*\}. \quad (11)$$

This completes our summary of the structure of our analysis. We now turn our attention to the means of generating the Green's function introduced in Eq. (10), and also comments are required on how the proper self-energy can be reduced to a form that is suitable for computation.

The next step is to construct the Green's function $D_{\Phi\Phi}(\vec{r},\vec{r}';\omega+i\eta)$, for the geometry of interest to us. To carry through a calculation of the proper self-energy, this is best accomplished by analytic methods. For this we need to develop a soluble model appropriate to the issues of interest to the present paper.

We begin by noting that a typical STM tip has a large radius of curvature, in the range of 10 nm or greater. Under typical experimental circumstances, the bottom ("south pole") of the tip is 5 Å (0.5 nm) from the adsorbate. Under these circumstances, we may model the tip as a large sphere, whose south pole is very close to the substrate. Our concern is with the zero-point electric field fluctuations in the very near vicinity of the south pole, and one may analyze these within the framework of this model with little error. Indeed, an explicit study[14] of STM tip/substrate plasmon enhancements of oscillating electric dipole under the tip shows their lateral range is limited to 3 or 4 nm; as discussed in this paper, the relevant length scale is $(Rd)^{1/2}$, with R as the radius of curvature of the tip and d as the distance of its south pole from the substrate. Many years ago, in an interesting and closely related physical context, it was shown that by using bispherical coordinates, one may describe the electrostatic response of a metallic sphere placed very close to a substrate.[15] We have employed the bispherical coordinate scheme more recently to discuss STM tip-induced enhancements of oscillating dipole moments on metallic surfaces[14,16] and also for discussions of aspects of the response of pairs of metallic nanospheres to laser radiation.[17,18]

Bispherical coordinates map the standard cylindrical coordinates (ρ, z, φ) onto a new set (β, α, φ). In the appendix of Ref. 16, one may find a summary of the transformations and a number of useful identities.[19] The surfaces of constant β are spheres with center on the z axis; when $\beta > 0$ the sphere lies in the upper half space, whereas when $\beta < 0$ the sphere lies in the lower half space. The surface $\beta = 0$ is the xy plane. We may thus easily describe a sphere placed above the xy plane in this coordinate system.

In the present work, we also wish to include the oxide layer onto which the molecules studied in Refs. 4, 5, and 24 are placed. Ideally we would like the oxide layer to be a perfectly flat film, with upper surface parallel to the xy plane and a small distance above it. This is very difficult to describe within the framework of the bispherical coordinate system. We have proceeded by modeling the oxide layer as bounded by a sphere of very large radius, with south pole 0.4 nm above the xy plane. When this is done, the oxide layer is not perfectly flat, but for quite a long distance from the origin of the xy plane its thickness varies little. Since the presence of the oxide layer is a rather modest influence on the nature of the electric field fluctuations near the origin of the xy plane, this approximation does not have a major influence on our quantitative results. We illustrate the geometry we use in Fig. 1.

To construct the function $D_{\Phi\Phi}(\vec{r}, \omega + i\eta)$, we begin by constructing the potential function we designate as $D_{\Phi\Phi}^{(0)}(\vec{r}, \vec{r}'; \omega + i\eta)$. This is the electrostatic potential of a single point charge of unit strength measured at $\vec{r}$ when the point charge is placed at point $\vec{r}'$. We will choose $\vec{r}'$ to lie in the vacuum region above the oxide layer, but below the STM tip. In this region, the dielectric constant $\epsilon(\vec{r}, \omega + i\eta)$ is equal to unity (ϵ_0), so in fact $D_{\Phi\Phi}(\vec{r}, \vec{r}'; \omega + i\eta)$ obeys the inhomogeneous differential equation in Eq. (10) everywhere, since the dielectric function is piecewise continuous and constant within each medium. Of course, it does not satisfy the ap-
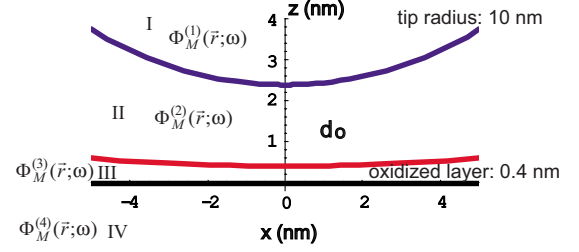

FIG. 1. (Color online) An illustration of the geometry utilized in the calculations described in the present paper. The metallic substrate lies in the lower half space $z < 0$, and then above this we have the oxide layer here modeled as a piece of surface of a sphere of very large radius. At the origin of the xy plane, the oxide layer is 0.4 nm thick. The STM tip is also modeled as a sphere, as illustrated. The functions $\Phi_M^{(i)}(\vec{r}, \omega)$ are the various pieces of the electrostatic potential $\Phi_M(\vec{r}, \omega)$ discussed in the text.

propriate boundary conditions at the various interfaces. We remark that in our various previous papers,[14,16–18] we have presented detailed discussions of how we synthesize electrostatic potentials in bispherical coordinates by matching the potentials and the appropriate derivatives at the various interfaces, so in the present paper we shall simply quote final results rather than summarize the lengthy algebra involved. If we define

$$\gamma_{l,m}(\beta', \alpha', \varphi') = \frac{\sqrt{\cosh \beta' - \cos \alpha'}}{c \cdot \epsilon_0} \frac{(l-m)!}{(l+m)!} P_l^m(\cos \alpha')$$
$$\times \exp[-im\varphi'], \qquad (12)$$

it then follows that

$$D_{\Phi\Phi}^{(0)}(\vec{r}, \vec{r}'; \omega + i\eta) = \sqrt{(\cosh \beta - \cos \alpha)} \sum_{l,m} \gamma_{l,m}(\beta', \alpha', \varphi')$$
$$\times \exp[-(l+1/2)|\beta - \beta'|] \cdot P_l^m(\cos \alpha)$$
$$\times \exp[im\varphi]. \qquad (13)$$

The right-hand side of Eq. (13) is quite simply the function $1/|\vec{r} - \vec{r}'|$ expressed in bispherical coordinates, with the point $\vec{r}$ given by (β, α, φ) and similarly for $\vec{r}'$. In Eq. (13), $P_l^m(x)$ is the associated Legendre function.

For brevity, we use in what follows ω in place of $\omega + i\eta$ and it is to be understood that ω is always chosen a bit above the real axis in the ω. We then add to $D_{\Phi\Phi}^{(0)}$ a function $\Phi_M(\vec{r}, \omega)$ which satisfies the homogeneous version of Eq. (10) everywhere. In each of the regions illustrated in Fig. 1, we may write $\Phi_M(\vec{r}, \omega)$ as a series expansion in the separable solutions of Laplace's equation in bispherical coordinates, which are of the form $\exp[\pm(l+1/2)\beta]P_l^m(\cos \alpha)\exp[im\varphi]$. For instance, in region II, which is the vacuum above the oxide layer and below the STM tip, we may write

$$\Phi_M(\vec{r}, \omega) = \Phi_M^{(2)}(\vec{r}, \omega) = \sqrt{\cosh \beta - \cos \alpha} \sum_{l,m} \{A_{lm} e^{-(l+1/2)\beta}$$
$$+ B_{lm} e^{(l+1/2)\beta}\} \cdot P_l^m(\cos \alpha) e^{im\varphi}. \qquad (14)$$

In Eq. (14), when the potentials and the appropriate combinations of derivatives are matched across the boundaries of

the various regions illustrated in Fig. 1, the coefficients A_{lm} and B_{lm} become functions of the combination β', α', and φ'. From the structure of the equations from which these coefficients are determined, one may show that one can write them in expansions of the form

$$A_{lm} = \sqrt{\cosh \beta' - \cos \alpha'} \sum_{l'=|m|}^{\infty} \{a_{lm}^{l'} e^{-(l'+1/2)\beta'} + b_{lm}^{l'} e^{(l'+1/2)\beta'}\} P_l^{-m}(\cos \alpha') e^{-im\varphi'}, \quad (15a)$$

and

$$B_{lm} = \sqrt{\cosh \beta' - \cos \alpha'} \sum_{l'=|m|}^{\infty} \{c_{lm}^{l'} e^{-(l'+1/2)\beta'} + d_{lm}^{l'} e^{(l'+1/2)\beta'}\} P_l^{-m}(\cos \alpha') e^{-im\varphi'}. \quad (15b)$$

The expressions in Eq. (15) allow us to write the Green's function in a form where every term in the series is separable in the variables (β, α, φ) and $(\beta', \alpha', \varphi')$. In region II of Fig. 1, which is the region where we want to describe the field fluctuations, we then have $D_{\Phi\Phi}(\vec{r}, \vec{r}'; \omega) = D_{\Phi\Phi}^{(0)}(\vec{r}, \vec{r}'; \omega) + \Delta D_{\Phi\Phi}(\vec{r}, \vec{r}'; \omega)$, where $\Delta D_{\Phi\Phi}(\vec{r}, \vec{r}'; \omega)$ is given by

$$\Delta D(\vec{r}, \vec{r}'; \omega) = [(\cosh \beta - \cos \alpha)(\cosh \beta' - \cos \alpha')]^{1/2} \sum_{l=0}^{\infty} \sum_{m=-l}^{+l} \sum_{l'=|m|}^{\infty} \{a_{lm}^{l'} e^{-(l+1/2)\beta} e^{-(l+1/2)\beta'} + b_{lm}^{l'} e^{-(l+1/2)\beta} e^{(l+1/2)\beta'}$$
$$+ c_{lm}^{l'} e^{(l+1/2)\beta} e^{-(l+1/2)\beta'} + d_{lm}^{l'} e^{(l+1/2)\beta} e^{(l+1/2)\beta'}\} \cdot P_l^m(\cos \alpha) P_{l'}^{-m}(\cos \alpha') e^{im(\varphi-\varphi')}. \quad (16)$$

When we calculate the spectral density function $\rho_{\Phi\Phi}(\vec{r}, \vec{r}'; \omega)$, only $\Delta D_{\Phi\Phi}(\vec{r}, \vec{r}'; \omega)$ contributes since $D_{\Phi\Phi}^{(0)}(\vec{r}, \vec{r}'; \omega)$ is real. With use of Eq. (16), the proper self-energy can then be written in the form

$$\Sigma_{\alpha,\alpha}(\varepsilon_\alpha) = -\frac{e^2}{\pi} \sum_\beta \int_0^\infty d\omega \left\{ \frac{f_\alpha}{(\varepsilon_\alpha - \varepsilon_\beta + \omega - i\eta)} + \frac{1 - f_\alpha}{(\varepsilon_\alpha - \varepsilon_\beta - \omega + i\eta)} \right\}$$
$$\cdot \mathrm{Im}\left[\sum_{l=0}^{l_{max}} \sum_{m=-l}^{l} \sum_{l'=|m|}^{l_{max}} \{a_{l,m}^{l'} I_{l,m;\alpha,\beta}^{(-)} I_{l',-m;\beta,\alpha}^{(-)} + b_{l,m}^{l'} I_{l,m;\alpha,\beta}^{(-)} I_{l',-m;\beta,\alpha}^{(+)} + c_{l,m}^{l'} I_{l,m;\alpha,\beta}^{(+)} I_{l',-m;\beta,\alpha}^{(-)} + d_{l,m}^{l'} I_{l,m;\alpha,\beta}^{(+)} I_{l',-m;\beta,\alpha}^{(+)}\} \right], \quad (17)$$

where

$$I_{lm;\mu\nu}^{(-)} = \int d^3r \varphi_\mu(\vec{r})^* \varphi_\nu(\vec{r}) \sqrt{\cosh \beta - \cos \alpha}$$
$$\times \exp[-(l+1/2)\beta] P_l^m(\cos \alpha) \exp[im\varphi], \quad (18a)$$

$$I_{lm;\mu\nu}^{(+)} = \int d^3r \varphi_\mu(\vec{r})^* \varphi_\nu(\vec{r}) \sqrt{\cosh \beta - \cos \alpha}$$
$$\times \exp[(l+1/2)\beta] P_l^m(\cos \alpha) \exp[im\varphi]. \quad (18b)$$

We conclude this section with comments on the numerical evaluation of the proper self-energy. Note, incidentally, that in the sum over β in Eq. (17), of course the term $\alpha = \beta$ is to be retained. If one applies the theory to the "sterile electron" mentioned in Sec. I, and the electron is above a simple planar dielectric, then the term with $\alpha = \beta$ just reduces to the classical image potential energy $-(e^2/4z_0)[(\epsilon_S - 1)/(\epsilon_S + 1)]$, where z_0 is the distance of the sterile electron above the substrate surface and ϵ_S is the static dielectric constant of the substrate. We refer the reader to Ref. 7 for a proof of this statement. The off-diagonal terms with $\alpha \neq \beta$ are contributions to the energy-level shift with origin in the dynamic nature of the zero-point fluctuations in the region outside the structure. These dynamic fluctuations produce virtual transitions to excited states, and the virtual fluctuations contribute

to the energy shift. Hence, as remarked in Sec. I, we refer to the energy-level shift contained in the proper self-energy as produced by a dynamic image potential. When the self-energy is calculated for an excited state with an empty state below it, then the imaginary part of the proper self-energy is nonzero. It is the imaginary part from which one can deduce the contribution to the nonradiative decay rate of the excited state from transfer of energy to the particle hole excitations of the surrounding media, or to surface plasmons if the transition energy falls in the appropriate energy range.

In the numerical evaluation of the proper self-energy, it is crucial to write the Green's function in a form where every term is separable, as in Eq. (16). The reason for this is that the general expression for the proper self-energy contains integrals over both $\vec{r}$ and $\vec{r}'$. It is extremely time-consuming to evaluate such six-dimensional integrals with accuracy sufficient to reliably compute the proper self-energy. Furthermore, each time the tip sample distance is changed, the large number of six-dimensional integrals must be recomputed if one uses Eq. (9). The separable form for the Green's function in Eq. (16) allows one to break the computation down into an evaluation of the sets of three-dimensional integrals defined in Eqs. (18). Notice the integrands in these expressions make no reference to the geometry of the system or to the material parameters of the constituents. Thus, given a set of orbitals sufficient in number to produce an adequate description of

the proper self-energy, the integrals in Eqs. (18) need to be computed only once and stored. They can then be called on repeatedly without any need to recomputed them, as one changes materials in the system, alters the tip/sample distance or any other feature.

The integrals in Eqs. (18) were evaluated on a cubic grid in Cartesian coordinates, with (β, α, φ) at each point in the grid determined from the coordinate transformation which relates the bispherical coordinates to their Cartesian equivalents. We used a total of 30 orbitals generated for the Mg porphine molecule in free space. The means by which these are calculated is described in Ref. 7. Plane-wave representations of the orbitals were kindly provided to us by J. X. Cao and Ruqian Wu. We found that very good convergence for the proper self-energy by cutting off the sums over l at l_{max} =8.

The calculations we report below assume the substrate is NiAl, with the experiments reported in Refs. 4, 5, and 24 in mind. Of course, we need both the real (ϵ_1) and the imaginary (ϵ_2) part of the dielectric constant of this material for our calculations. While there are a number of papers in the literature which report data on $\epsilon_2(\omega)$, and compare the data with results generated from electronic structure calculations on NiAl,[20] there are no published data on the real part, $\epsilon_1(\omega)$. The data on $\epsilon_2(\omega)$ do not extend over a wide enough frequency range to allow $\epsilon_1(\omega)$ to be constructed from a Kramers Kronig transform. We have learned[21] that Joo Yull Rhee has measured both the $\epsilon_1(\omega)$ and $\epsilon_2(\omega)$ for NiAl, and he has kindly supplied us with his data. The data extend from 0.5 to 5.5 eV, so our integrations over frequency in Eq. (17) have been confined to this range. It is difficult to do a meaningful extrapolation of the data to higher frequencies, unfortunately. It would be of great interest to calculations such as those reported here to have data on the dielectric response of NiAl to much higher frequencies. In the absence of such data, we have had to limit our frequency integration to the range we discussed. This limitation has no influence on our calculation of the nonradiative lifetime, notice.

III. NUMERICAL RESULTS

In this section, we present the results of our numerical studies. We begin with a discussion of the nature of the electric field fluctuations near the sample surface, and the influence of the STM tip on the fluctuation spectrum. In what follows, we shall present results for the spectral density function $\rho_{\Phi\Phi}(\vec{r}, \vec{r}'; \Omega)|_{r=r'}$, which provides us with the frequency spectrum of the fluctuations in the electrostatic potential at point $\vec{r}$. The results we present will focus on the line between the "south pole" of the tip, and the point on the oxide surface just under the south pole of the tip.

We first remark that in all the results presented in the present section, we assume an oxide layer is present on the sample surface, with the thickness of 0.4 nm. Of course, we have no detailed information on the optical properties of the oxide layers which are present on the samples probed experimentally, so in our numerical work we have taken the dielectric constant of the oxide layer to be independent of frequency, real and we take its value $\epsilon_{ox}=4$. This value is

typical of many wide gap insulating oxides. The precise value of the dielectric constant in the oxide layer has only a modest quantitative influence on our results for the energy-level shifts and nonradiative lifetimes discussed further on in this section. In all the calculations presented below, we have also taken the radius of curvature of the tip to be 10 nm, which we understand is typical of those used in the experiments we shall discuss.

In Fig. 2(a), we show the spectrum of potential fluctuations at the outer surface of an oxide layer on a Ag surface, in the absence of the STM tip. Also shown is the spectrum 0.5 nm above the oxide surface. The dominant peak in the curve is near below 3.5 eV very close to the surface plasmon peak on the clean Ag surface. We remark that in all of our calculations that incorporate Ag in either the tip or substrate, we have employed the dielectric constant measured some years ago by Johnson and Christy.[22] The structures we see in Fig. 2(a) are broadened a bit by the presence of the oxide layer, which introduces some dispersion into the surface plasmon. In the next paragraph, we elaborate in this remark.

The structure of the two spectra in Fig. 2(a) may be understood from the following physical argument. Suppose for the moment we model the Ag substrate with the simple model dielectric constant $\epsilon_{Ag}(\omega) = \epsilon_\infty - (\omega_P/\omega)^2$. In the absence of the oxide layer, and within the framework of the electrostatic theory used here, the Ag surface supports a surface plasmon whose frequency is independent of the wave vector $Q_\parallel$ parallel to the surface. Its frequency is $\omega_{SP}^{(Ag)} = \omega_P/(\epsilon_\infty + 1)^{1/2}$. The presence of the oxide layer introduces dispersion into the surface plasmon. If the thickness of the oxide layer is d, then if $Q_\parallel$ is the two-dimensional wave vector of the surface plasmon, when $Q_\parallel d < 1$ the surface plasmon frequency approaches $\omega_{SP}(Q_\parallel) \approx \omega_{SP}^{(Ag)}$. In the large wave vector regime $Q_\parallel d > 1$, it approaches the lower frequency $\omega_{SP}(Q_\parallel) \approx \omega_{SP}^{(Ag+ox)} = \omega_P/(\epsilon_\infty + \epsilon_{ox})^{1/2}$. Thus, the oxide layer produces a redshift in the surface plasmon frequency at large wave vectors. Right at the oxide surface, the large wave vector plasmons contribute to the spectrum of potential fluctuations, and the spectrum extends down to about 3.2 eV, which is $\omega_{SP}^{(Ag+ox)}$. Now as one moves into the vacuum above the oxide layer, the contribution from the large wave vector modes is suppressed, as evidenced by the asymmetric peak calculated 0.5 nm above the surface. To appreciate why this is so, recall that the electrostatic potential associated with a surface plasmon of wave vector $Q_\parallel$ fall off as $\exp(-Q_\parallel z)$. For the planar surface with oxide layer present, of course, a plane-wave representation such as that utilized in our earlier paper[7] could be used to generate the result in Fig. 2(a). We see that the bispherical coordinate description employed here nicely generates results appropriate to the flat surface, if enough l values are included to achieve convergence. We have found that using $l_{max}=8$ produces satisfactory results, as noted above.

In Fig. 2(b), we show calculations for the case where a Ag tip is 1 nm from the oxide covered Ag surface. The solid line shows the spectral density function evaluated on the outer surface of the oxide, just under the south pole of the tip. We see a mode structure which extends below 3 eV. We now have a surface plasmon spectrum wherein the modes are coupled modes of the tip/substrate/oxide system. As dis-
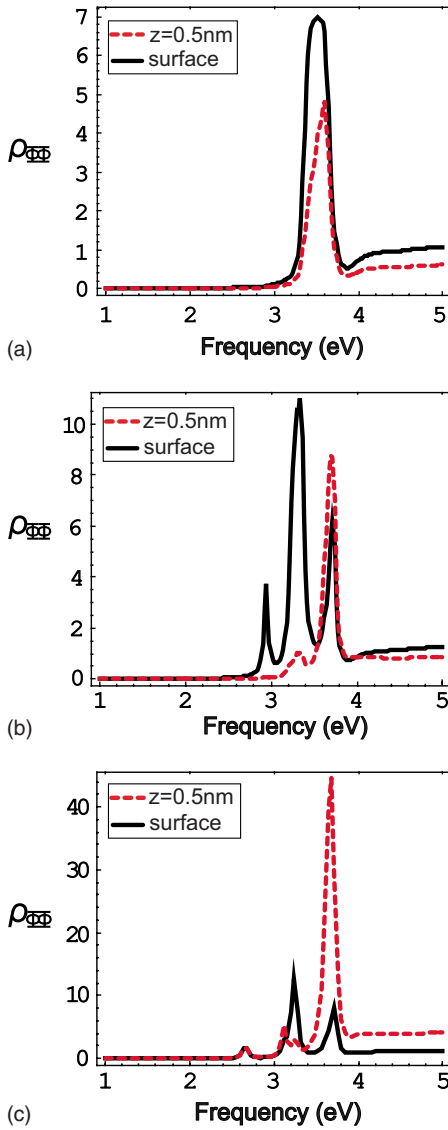
(a)

(b)

(c)

FIG. 2. (Color online) We show calculations of the spectral density function $\rho_{\Phi\Phi}(\vec{r},\vec{r};\Omega)$ for a Ag tip near an oxidized Ag surface. The oxide layer is 0.4 nm thick. In (a) we show the spectral density for a point on the surface of the oxide layer (solid curve), with tip absent, and the dotted curve is the spectral density 0.5 nm above the oxide surface. In (b), the tip is 1 nm from the surface of the oxide. The solid line is the spectral function evaluated at the oxide surface just under the south pole of the tip, and the dotted line is the spectral function evaluated 0.5 nm above the oxide layer, just under the tip. (c) is the same as (b) but now the tip is 0.5 nm from the substrate Thus, the dotted line gives the spectrum of fluctuations just at the bottom of the tip. The units of $\rho_{\Phi\Phi}$ are arbitrary, but the same convention is used for all three figures and in the figures that follow.

cussed earlier,[12] there are modes trapped under the tip, in a spatial regime whose spatial extent is the length scale $(RD)^{1/2}$, where R is the radius of curvature of the tip and D is a measure of the tip/substrate separation. There are modes of acoustical character trapped in this region, and modes of optical character. The low frequency feature is produced by standing wave acoustic modes, and the high frequency structure by standing wave optical modes. The dotted line in Fig.
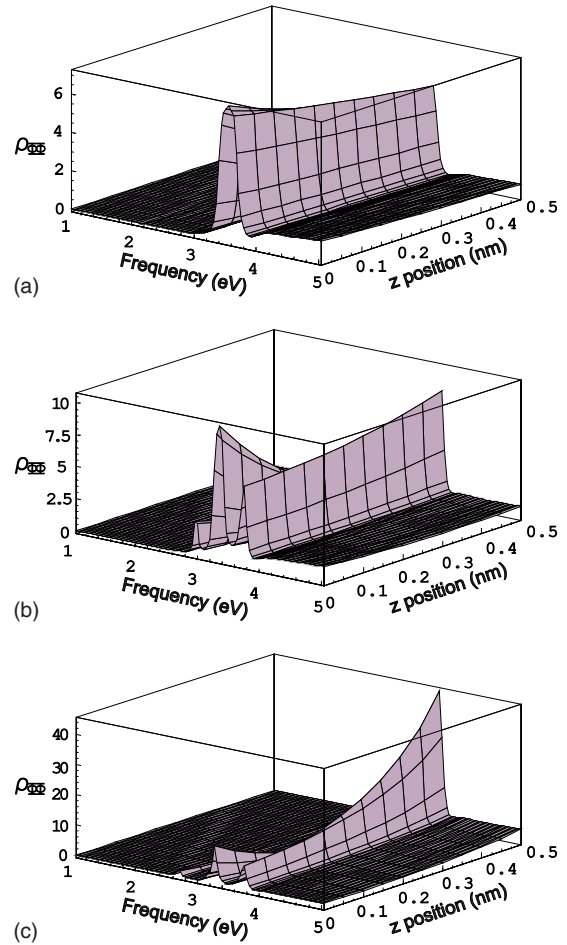

(a)

(b)

(c)

FIG. 3. (Color online) Calculations of the spectral density function $\rho_{\Phi\Phi}(\vec{r},\vec{r};\Omega)$ as a function of distance from a point on the oxide covered Ag surface, to the Ag tip for three cases: (a) the tip is infinitely far from the substrate, (b), the tip is 1 nm from the oxide surface, and (c) the tip is 0.5 nm from the oxide. The units of $\rho_{\Phi\Phi}$ are arbitrary, but as in Fig. 2 the same units are used for all three panels.

2(b) is the spectral function evaluated 0.5 nm above the oxide surface, halfway to the south pole of the tip. This spectral density is dominated by the contribution from the Ag plasmon localized near the bottom of the tip, and the two low frequency modes are suppressed. Clearly these low frequency modes have eigenvectors rather localized to the oxide/substrate combination. In Fig. 2(c), we provide the same information as in Fig. 2(b), but now the tip is 0.5 nm from the substrate. Thus, the dotted curve is the fluctuation spectrum right at the south pole of the tip. Finally in Fig. 3 we show how the spectrum of electrostatic potential fluctuations varies as one moves from the point on the oxide surface just under the tip, upward to the south pole of the tip itself.

Our conclusion is that the Ag surface is highly "surface plasmon active." This is well known, of course though we see in Figs. 2 and 3 the role of the oxide layer and the STM tip on the potential fluctuations in the region of interest. As one brings the Ag tip closer to the surface, there are substantive changes in the spectrum of the electrostatic potential fluctuations. In the present paper, we have presented results

only along the line between the south pole of the STM tip and the substrate just below. We remark that in an earlier paper,[18] for the closely related case of two nearby dissimilar spheres we have provided studies of the angular variation in the plasmon enhancement effects and the lateral extent of the enhancement effects on the surface below the tip can be found in our previous studies.[23] Calculations of these effects for the system studied here will be very similar to the results just cited.

The calculations explored in the present paper were motivated by the experiments reported in Refs. 4 and 5. The measurements were carried out on an oxidized NiAl surface. We next present spectral density calculations for a Ag tip near the oxidized NiAl surface. For these calculations, we require both the real and imaginary parts of the optical dielectric constant for NiAl, of course. As discussed in Sec. II, there is no data in the literature on the real part of the dielectric constant of this material. We have used data kindly supplied to us by Joo Yull Rhee, as noted in Sec. II.

In Fig. 4(a), we show the spectral density of electrostatic potential fluctuations at the surface of the oxidized NiAl surface, when the tip is infinitely far away. One may notice two things in these results. First of all, we see no evidence of a sharp structure that one may associate with a surface plasmon for this material. The reason is that NiAl is very lossy indeed, and no long-lived surface plasmon is supported by the surface of this material. Second, we see that the magnitude of $\rho_{\Phi\Phi}$ is rather small, so the amplitude of the zero-point fluctuations in the electrostatic potential are rather small near this surface. On the oxidized surface, the large wave vector surface plasmon frequency is given by the condition $\epsilon_1^{(NiAl)}(\omega) = -4$. This condition is satisfied for a frequency near 1.8 eV, for NiAl. At this frequency, $\epsilon_2^{(NiAl)}(\omega) \approx 10$, and the mode is damped so heavily that we see no sharp resonant structure near this frequency in Fig. 4(a). There is a very broad peak in the spectrum in this spectral region, but it sits on a large background and this cannot be thought of as produced by a well defined, long-lived surface plasmon. In contrast, for Ag, the condition $\epsilon_1^{(Ag)}(\omega) = -4$ is satisfied near 3.2 eV, and in this vicinity $\epsilon_2^{(Ag)}(\omega) \approx 0.3$, smaller by a factor of 30 than the case of NiAl. In Fig. 5(a), as in Fig. 3(a), we show the spectrum of electrostatic potential fluctuations as one moves away from the oxide surface. Clearly, the NiAl surface, clean or oxidized, is a "dead surface" from the perspective of its ability to support surface plasmons.

As we bring a Ag tip near the NiAl surface, we barely see the imprint of the Ag tip surface plasmon on the spectrum of potential fluctuations near the oxide surface. We see this in Fig. 4(b) and in Fig. 4(c). However, as one moves 0.5 nm above the oxide surface, with the tip 1 nm above it, from Fig. 4(b) one sees the clear imprint of the plasmon localized on the Ag tip. Thus, when we explore the influence of the electrostatic potential fluctuations on the Mg porphine molecule, the portion of the electron density very close to the oxide surface is only modestly influenced by the presence of the Ag tip plasmon, but in the upper reaches of the molecule the electron density will sense the presence of this mode.

We next turn to our studies of the energy-level shifts produced by the dynamic image potential, and also the nonradi-
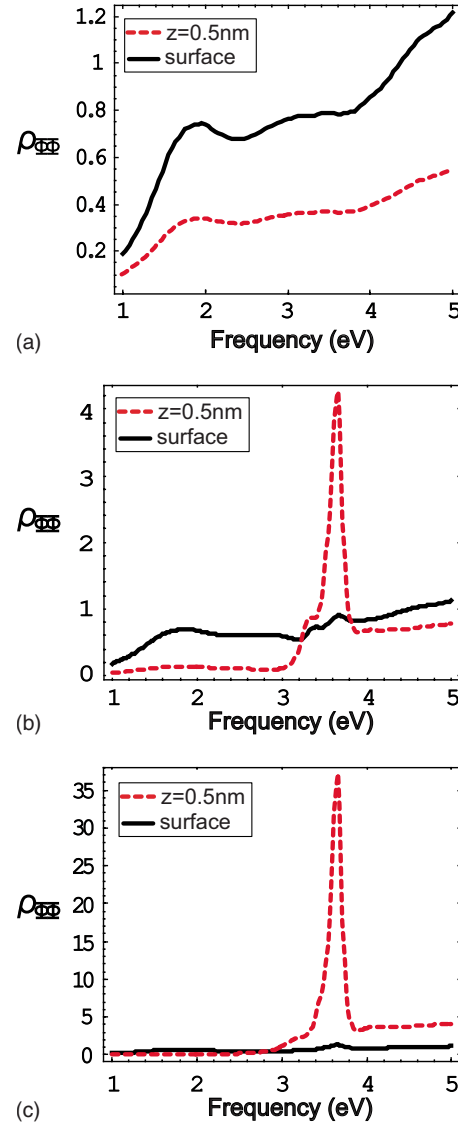

FIG. 4. (Color online) The same as Fig. 2, but now the oxidized Ag substrate has been replaced by an oxidized NiAl substrate. In (a), the tip is infinitely far away, in (b) it is 1 nm away from the oxide, and in (c) it is 0.5 nm away from the oxide. In all three panels, the dotted line shows the spectrum of potential fluctuations 0.5 nm above the oxide surface.

ative decay rate of excited states. With the experiments of Refs. 4 and 5 in mind, we have chosen to explore the Mg porphine molecule placed on the oxidized NiAl surface. We shall then examine the influence of various tip materials on these properties.

As outlined above, our task is to evaluate the proper self-energy whose form is given in Eq. (17). The energy-level shifts produced by the dynamic image potential are obtained from the real part of the proper self-energy, and the nonradiative lifetime of excited states is found by evaluating the imaginary part. One should note that the sum over intermediate states in Eq. (17), denoted by the sum over β, includes the diagonal term in which $\beta = \alpha$ and then in the energy denominator $\varepsilon_\beta = \varepsilon_\alpha$. As discussed in Ref. 7, it is possible to use a sum rule to evaluate the integral over the frequency ω
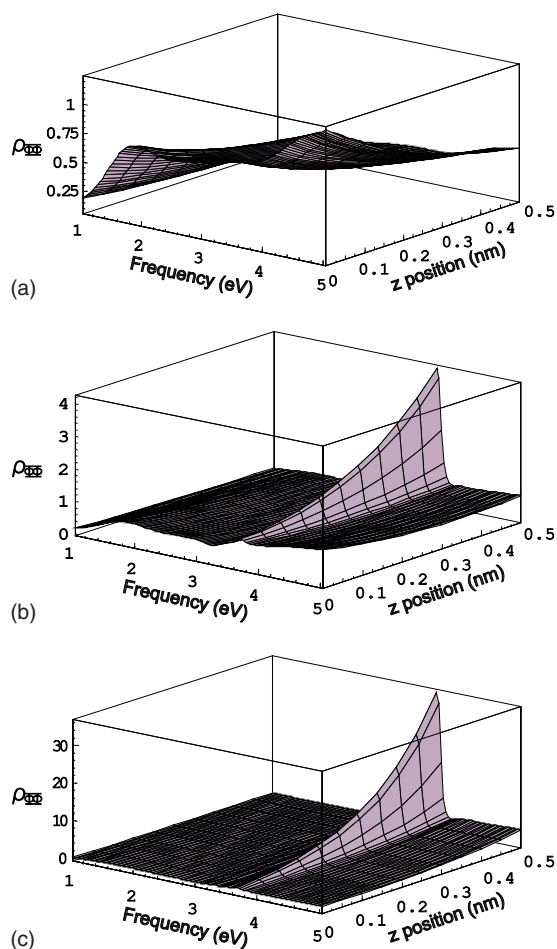
FIG. 5. (Color online) The same as Fig. 3, but now the oxidized Ag substrate has been replaced by an oxidized NiAl substrate.

in Eq. (17). The resulting form involves only the static dielectric constants of the various constituents. The use of the sum rule greatly simplifies the evaluation of the diagonal term. We have not presented the details of how this is done in the present paper, but in Ref. 7 a derivation is presented for the case where the tip is not present.

The wave functions we have used to characterize the molecule are those which were generated for the calculations discussed in Ref. 7. The reader will find a summary of the electronic structure calculation in this paper. In the sum over intermediate states, we have included a total of 30 states, as in Ref. 7. In evaluating the matrix elements in Eq. (17) of the present paper, we have employed a rectangular grid which covered a rectangular prism with a square base of 2 nm, and a height of 1 nm. The grid of points was $180 \times 180 \times 90$ in size. We found this provides good convergence. In the sums over the angular momentum variable l, as mentioned earlier we retained all terms up to $l_{max} = 8$.

For the Mg porphine molecule on the oxidized NiAl surface, we summarize our calculations of the energy-level shifts induced by the dynamic image potential in Fig. 6, for four of the principal orbitals of the molecule. We consider three tip materials, Ag, Au, and W. We remark that we have done calculations for a Cu tip as well, and the results are very similar to the Ag and Au results, save for small quanti-
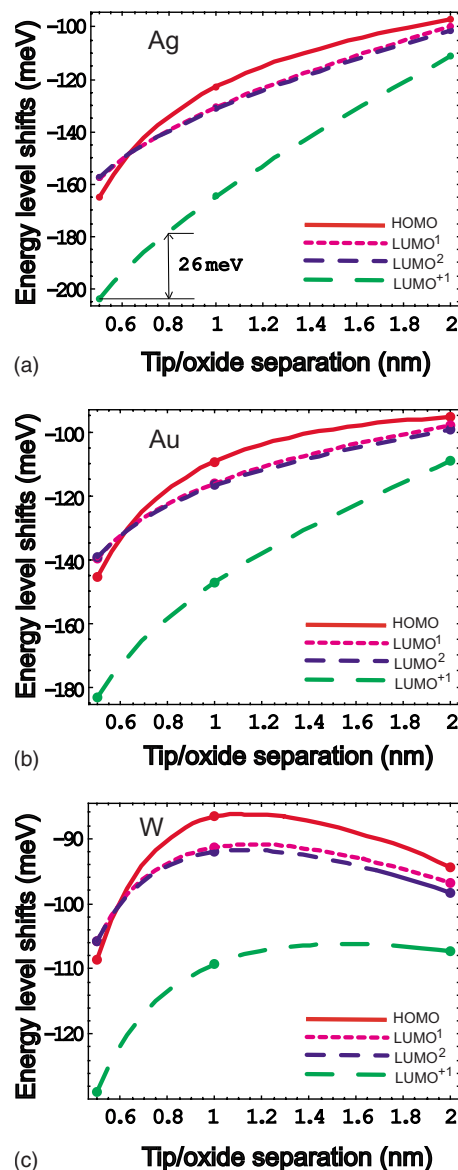

FIG. 6. (Color online) For four principal energy levels of the Mg porphine molecule adsorbed on the oxidized NiAl surface, we show the tip-induced energy-level shifts, with origin in the modification of the dynamic image potential as the STM tip approaches the molecule. We consider tips fabricated from four materials, (a) Ag, (b) Au, and (c) W.

tative differences. The lowest unoccupied molecular orbital (LUMO) state of this molecule is twofold degenerate when the molecule is in free space, and so far as we can tell from our calculations these two states remain degenerate or very nearly so as the tip is brought down to the surface.

In the case of the Ag tip, when the tip is very far from the substrate, then the dynamic image potential shift has its origin in the charge fluctuations in the substrate/oxide system. We find that with the tip far away, all of the orbitals are shifted by very close to the same amount, in the 108–110 meV range. In Ref. 7, the calculations which were presented considered this case only. The results presented there show that the dynamic image potential shift for all four orbitals was very close to the same with the tip absent, however the

shifts were found to be smaller (65–66 meV) than the results presented in the present paper. It is our view that there may have been an issue of convergence in the earlier work. We have checked the results of the present calculations as follows. First of all, with the tip far away we have calculated the dynamic image potential energy-level shifts through use of the bispherical coordinates described in the present paper. In Ref. 7, for the case where the tip is absent, a very different plane-wave description of the potential fluctuations was utilized. During the course of our present study, we have carried out calculations with the plane-wave representation as well, and we find very good agreement with the results generated by use of the bispherical coordinates.

In Ref. 24, data are presented on the shift in the energy of the LUMO+1 state of the Mg porphine molecule, as the STM tip is moved from 0.8 nm above the surface, to 0.5 nm. It is found experimentally that this level shifts by 30 meV. As one sees from the inset in Fig. 6(a), our calculation suggests the shift should be 26 meV. We regard the agreement between the theory and the data to be very excellent indeed. In our view, this agreement establishes that the tip modulated dynamic image potential shifts explored in the present paper are the dominate source of tip-induced shifts in the energy levels of this molecule.

Of considerable interest are the calculations for the W tip displayed in Fig. 6(c). Notice that as the tip is brought down, initially the energy levels rise a bit, rather than drop in energy as one would expect if the energy-level shifts were controlled by the elementary static image potential of dielectric theory. This shows that the virtual transitions described by the terms with $\beta \neq \alpha$ play a role in the real part of the proper self-energy. It is not necessarily the case that the energy levels all lower as the tip approaches the molecule, if there are intermediate states that contribute importantly to the proper self-energy. The dynamic aspect of the image potential asserts itself through such terms.

We see from Fig. 6 that as the STM tip is brought toward the molecule probed, the energies associated with the various orbitals shifts appreciably. Clearly one must keep the presence of such shifts in mind, when comparing electronic structure calculations with spectroscopic data generated by scanning tunneling microscopy. For the case we consider, the dynamic image potential shift is in the range of 100 meV for all orbitals, and it can increase to 200 meV as the tip comes close enough to the molecule to perform spectroscopic studies. Corrections such as these must be included in density-functional studies of adsorbate energy levels on substrates, under conditions where direct hybridization between the electrons in the adsorbate and in the substrate may be neglected.

In the experiments reported in Refs. 4 and 5, when electrons are injected into the LUMO+1 level of the Mg porphine molecule, a photon is detected. This is associated with the transition from the LUMO+1 level, down to the doubly degenerate LUMO states. In Fig. 7, we show our calculation of the energy of the emitted photon, as a function of distance of the tip from the molecule. Despite the large shifts experienced by both the LUMO+1 state and the LUMO states, in fact the energy difference between them does not change greatly for the range of tip/molecule separations considered.
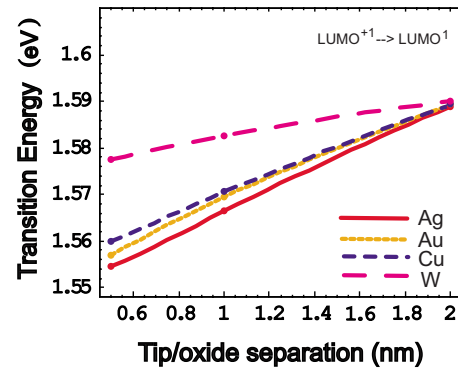

FIG. 7. (Color online) For the Mg porphine molecule on the oxidized NiAl surface, we show our calculation of the energy of the photon emitted in the transition from the LUMO+1 state to the LUMO states, as a function of the distance of the tip above the oxide surface. The energy-level separation between these two states, for the molecule in free space, is taken from the electronic structure calculation reported in Ref. 4.

Basically the two states experience rather similar energy shifts, with the consequence that the energy of the emitted photon depends only slightly on the tip/molecule distance. This conclusion is compatible with the data in Refs. 4 and 5. We remark that to produce Fig. 7, we have used the LUMO+1/LUMO energy separation (1.6 eV) for the molecule in free space which results from an electronic structure calculation reported in Ref. 4. This provides a frequency for the emitted photon in excellent accord with the observations, when our dynamic image potential level shifts are included. The electronic structure calculations reported in Ref. 7 give a somewhat smaller energy difference. The principal point illustrated in Fig. 7 is the relative insensitivity of the energy of the emitted photon to the tip/molecule separation, and the absolute value of the energy is of less importance.

We have also calculated the nonradiative lifetime of the LUMO+1 state of the Mg porphine molecule on the oxidized NiAl surface and its dependence on the distance of the tip from the oxide layer. The physical process is decay of the excited electron from the LUMO+1 state to the LUMO manifold, with the energy transferred to the electrons in the NiAl substrate via the coupling provided through the fluctuations in the electrostatic potential. As we see in Fig. 8, as the tip is brought closer to the oxide layer, the nonradiative lifetime decreases substantially. Notice that for the case of the Ag tip, the transition energy of 1.55 eV is far below the plasmon structure of Ag, as we can appreciate from our earlier discussion. We have also seen that the NiAl surface itself is "dead" insofar as supporting surface plasmons is concerned. Thus, the nonradiative lifetime has its origin with transfer of energy to particle hole pairs in the substrate/tip combination as opposed to surface plasmons. It is interesting that the nonradiative lifetimes calculated for noble metal tips are all quite similar in magnitude, while that for a W tip is considerably shorter. It is the case that W is also a very lossy material in this frequency range, so the presence of the W tip adds access to a new channel of decay in which the density of particle hole pair states is large. We remark that if we compare the results in Fig. 8 with those of Ref. 7 when the
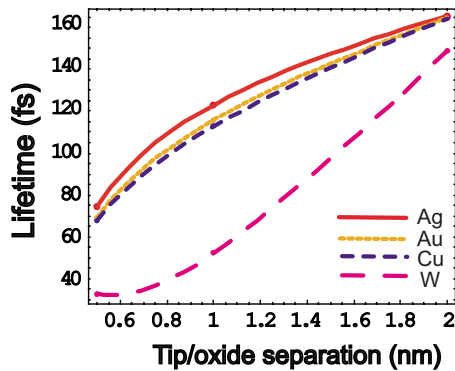
FIG. 8. (Color online) The nonradiative lifetime for a Mg porphine molecule on the oxidized NiAl surface, as a function of the distance of the STM tip from the oxide layer. Various tip materials are considered, as indicated in the inset.

tip is far from the substrate, the nonradiative lifetime we find in the present calculations is longer than that reported earlier by roughly a factor of 2. It is our view that convergence issues in the earlier calculations are responsible for this discrepancy, as noted above.

We can compare the results in Fig. 8 with data reported in Ref. 5, where a Ag tip was employed with the Mg porphine molecule on the oxidized NiAl surface. These authors find the nonradiative lifetime of the LUMO+1 state to be 220 fs (3 meV), while from Fig. 8 our calculated lifetime is somewhat shorter, in the range of 90 fs for the appropriate tip/oxide separation. Surely the theory and experimental data are close enough for one to argue that the mechanism explored here indeed controls the nonradiative lifetime. Calculations such as ours are based on an idealized geometry, of course. For instance, it is not clear how the geometry of the STM tip corresponds to our use of a perfectly spherical shape for the tip.

IV. CONCLUDING REMARKS

In this paper we have presented studies of the frequency spectrum of electrostatic potential fluctuations near oxidized metallic substrate, with emphasis on the influence of a nearby STM tip on the frequency spectrum of such fluctuations. We see that the presence of the tip leads to substantial changes in the nature of these fluctuations.

Our studies of the energy-level shifts of four of the principal states of the Mg porphine molecule placed on the oxidized NiAl(110) surface show that the energy-level shifts which result from the interaction of the potential fluctuations just described are appreciable, in the range of 100–200 meV, depending on the distance of the tip from the oxide layer. These results establish the importance of including corrections from the dynamic image potential on energy-level positions if one wishes to place results from electronic structure calculations alongside of data, for adsorbates placed on oxidized surfaces. The very good agreement between our calculated energy-level shift of the LUMO+1 level and the data of Ref. 24 as the distance between the STM tip and the oxide layer is further evidence that the level shifts explored here are indeed present. It is the case as well that the nonradiative lifetime of the LUMO+1 state we calculate is rather close to the experimental value. It is difficult to make precise comparisons between our calculations and the data, because it is not entirely clear that the geometry of the particular tip used in the measurements conforms to our model description. With this uncertainty in mind, we regard the agreement between theory and experiment to be very satisfactory.

ACKNOWLEDGMENTS

*pingc@uci.edu

†dlmills@uci.edu

[1] B. C. Stipe, M. A. Rezaei, and W. Ho, Science **280**, 1732 (1998).

[2] L. J. Lauhon and W. Ho, Phys. Rev. Lett. **85**, 4566 (2000).

[3] H. J. Lee, W. Ho, and M. Persson, Phys. Rev. Lett. **92**, 186802 (2004); T. M. Wallis, N. Nilius, and W. Ho, J. Chem. Phys. **119**, 2296 (2003).

[4] S. W. Wu, N. Ogawa, and W. Ho, Science **312**, 1362 (2006).

[5] S. W. Wu, G. V. Nazin, and W. Ho, Phys. Rev. B **77**, 205430 (2008).

[6] A comparison between energy-level widths for C60 molecules adsorbed on the unoxidized NiAl(110) surface and C60 adsorbed the oxidized NiAl(110) surface is found in N. A. Pradhan, N. Liu, and W. Ho, J. Phys. Chem. B **109**, 8513 (2005).

[7] D. L. Mills, J. X. Cao, and Ruqian Wu, Phys. Rev. B **75**, 205439 (2007).

[8] As examples, see M. Heinrichsmeier, A. Fleszar, W. Hanke, and A. G. Eguiluz, Phys. Rev. B **57**, 14974 (1998); and M. Dion, H. Rydberg, E. Schroder, D. C. Langreth, and B. I. Lundqvist, Phys. Rev. Lett. **92**, 246401 (2004).

[9] D. L. Mills, Surf. Sci. **48**, 59 (1975); see H. Ibach and D. L. Mills, *Electron Energy Loss Spectroscopy and Surface Vibrations* (Academic, San Francisco, 1982), Chap. 3.

[10] D. L. Mills, R. B. Phelps, and L. L. Kesmodel, Phys. Rev. B **50**, 6394 (1994).

[11] As we shall see in the discussion presented in Sec. III, the calculations presented in the present paper suggest the numerical results stated in Ref. 7 are not quite correct, possibly because of convergence issues. However, our results are not far from those presented earlier so the general conclusions of Ref. 7 remain unchanged.

[12] D. L. Mills, Phys. Rev. B **65**, 125419 (2002); Shiwei Wu and D. L. Mills, *ibid.* **65**, 205420 (2002).

[13] A. A. Abrikosov, L. P. Gor'kov, and I. E. Dzyaloshinskii, *Methods of Quantum Field Theory in Statistical Physics* (Prentice-Hall, Englewood Cliffs, NJ, 1963), Chap. 6.

[14] Shiwei Wu and D. L. Mills, Phys. Rev. B **65**, 205420 (2002).

[15] R. W. Rendell, D. J. Scalapino, and B. Muhlschlegel, Phys. Rev. Lett. **41**, 1746 (1978).

[16] D. L. Mills, Phys. Rev. B **65**, 125419 (2002).

[17] Ping Chu and D. L. Mills, Phys. Rev. Lett. **99**, 127401 (2007); see the erratum, Ping Chu and D. L. Mills, *ibid.* **100**, 059901(E) (2008).

[18] Ping Chu and D. L. Mills, Phys. Rev. B **77**, 045416 (2008).

[19] The reader should note that on the right-hand side of Eq. (A3) in Ref. 16, the quantity $c^2 \sin^2 \alpha$ should be replaced by $c^2/\sin^2 \alpha$.

[20] For a discussion of the real part of the optical conductivity of FeAl, NiAl, and CoAl and a comparison between theory and experiment, see J. Y. Rhee, J. Korean Phys. Soc. **43**, 1091 (2003).

[21] D. W. Lynch (private communication).

[22] P. B. Johnson and R. W. Christy, Phys. Rev. B **6**, 4370 (1972).

[23] See the second of the two papers cited in Ref. 12.

[24] G. V. Nazin, S. W. Wu, and Wilson Ho, Proc. Natl. Acad. Sci. U.S.A. **102**, 8832 (2005). The data discussed in the text are found in Fig. 4(c) of this paper.